Observed covariance between ecosystem carbon exchange and atmospheric boundary layer dynamics at a site in northern Wisconsin

C. Yi,[1,2] K. J. Davis,[1] P. S. Bakwin,[3] A. S. Denning,[4] N. Zhang,[4] A. Desai,[1] J. C. Lin,[5] and C. Gerbig[5]

Received 19 September 2003; revised 18 February 2004; accepted 2 March 2004; published 17 April 2004.

[1] Ecosystem CO_2 exchange and atmosphere boundary layer (ABL) mixing are correlated diurnally and seasonally as they are both driven by solar insulation. Tracer transport models predict that these covariance signals produce a meridional gradient of annual mean CO_2 concentration in the marine boundary layer that is half as strong as the signal produced by fossil fuel emissions. This rectifier effect is simulated by most global tracer transport models. However, observations to constrain the strength of these covariance signals in nature are lacking. We investigate the covariance between ecosystem carbon dioxide exchange and ABL dynamics by comparing one widely cited transport model with observations in the middle of the North American continent. We measured CO_2 flux and mixing ratio using an eddy-covariance system from a 447-m tower in northern Wisconsin, mixed layer depths using a 915-MHz boundary layer profiling radar near the tower, and vertical CO_2 profiles from aircraft in the vicinity of the tower. We find (1) that simulated and observed net daily CO_2 fluxes are similar; (2) the simulated maximum ABL depths were too shallow throughout year; (3) the simulated seasonal variability of the CO_2 mixing ratio in the lowest layer of the free troposphere is 3 ppm smaller than that inferred from a mixed layer jump model and boundary layer observations; and (4) the simulated diurnal and seasonal covariance between CO_2 flux and mixing ratio are weaker than the observed covariance. The comparison between model and observations is limited by the questionable representativeness of a single observing site and a bias towards fair weather observing conditions. *INDEX TERMS:* 0315 Atmospheric Composition and Structure: Biosphere/atmosphere interactions; 3307 Meteorology and Atmospheric Dynamics: Boundary layer processes; 3322 Meteorology and Atmospheric Dynamics: Land/atmosphere interactions; 3379 Meteorology and Atmospheric Dynamics: Turbulence; *KEYWORDS:* terrestrial CO_2 fluxes, atmospheric boundary layer dynamics, global change

Citation: Yi, C., K. J. Davis, P. S. Bakwin, A. S. Denning, N. Zhang, A. Desai, J. C. Lin, and C. Gerbig (2004), Observed covariance between ecosystem carbon exchange and atmospheric boundary layer dynamics at a site in northern Wisconsin, *J. Geophys. Res.*, *109*, D08302, doi:10.1029/2003JD004164.

1. Introduction

[2] The influence of terrestrial CO_2 exchange on the distribution of CO_2 in the atmosphere is modulated by the dynamics of the atmospheric boundary layer (ABL). On summer days the depletion of CO_2 due to photosynthetic uptake is diluted by deep convective mixing, while at night, CO_2 from respiration accumulates near the surface in a shallow, stable ABL. Outside of the tropics, a similar covariance occurs over seasonal scales, i.e., the net ecosystem-atmosphere exchange (NEE) of CO_2 is generally negative (uptake) in summer and positive in winter, combined with deeper mixing in summer. The covariance between terrestrial CO_2 exchange and vertical mixing influences the time-mean vertical partitioning of CO_2 between the ABL and free troposphere (FT) [*Denning et al.*, 1995].

[3] Atmospheric inversion calculations infer the distribution of surface sources and sinks from distributions of CO_2 observed at a network of air sampling stations primarily located in the marine boundary layer (MBL) [*Tans et al.*, 1990]. Most tracer transport models [*Denning et al.*, 1996a, 1996b; *Law and Simmonds*, 1996; *Law and Rayner*, 1999; *Bousquet et al.*, 2000] used for these calculations predict elevated concentrations of CO_2 at MBL stations downwind of the temperate continents due to rectification of purely seasonal exchange with terrestrial biota (i.e., CO_2 exchange with a zero annual mean at each model grid cell). This rectification enhances the simulated annual mean north-

[1]Department of Meteorology, Pennsylvania State University, University Park, Pennsylvania, USA.
[2]MOE Key Laboratory of Environmental Change and Natural Disaster, IRS, Beijing Normal University, Beijing, China.
[3]NOAA Climate Monitoring and Diagnostics Laboratory, Boulder, Colorado, USA.
[4]Department of Atmospheric Science, Colorado State University, Fort Collins, Colorado, USA.
[5]Department of Earth and Planetary Sciences, Harvard University, Cambridge, Massachusetts, USA.

0148-0227/04/2003JD004164$09.00

south CO_2 gradient and, since observations show only a modest north-south gradient [*Tans et al.*, 1990; *Conway et al.*, 1994], the difference implies a larger compensating temperate sink in the inverse calculations. The strength of this rectifier effect on the simulated annual mean Arctic-to-Antarctic difference in the MBL varies from slightly negative to more than 2.5 ppm among different transport models [*Law et al.*, 1996] and is one of the largest sources of uncertainty in estimates of continental-scale carbon fluxes [*Gurney et al.*, 2002, 2003]. The covariance between ecosystem CO_2 fluxes and the ABL dynamics drives the rectifier effect. Observations to constrain the strength of the rectifier effect in nature are lacking. Continuous observations of NEE of CO_2 (e.g., FLUXNET) [*Baldocchi et al.*, 2001] combined with long-term continuous measurements of ABL structure using boundary layer profiling radar [*Ecklund et al.*, 1988; *Angevine et al.*, 1998] can provide the data that is needed to assess the covariance.

2. Materials and Methods

2.1. Site and Measurements

[4] The study site is located in Chequamegon National Forest in northern Wisconsin (45.95°N, 90.27°W; elevation 473 m). The region is in a heavily forested zone of low relief. The tower is a 447 m tall television transmitter surrounded by a grassy clearing of about 180 m radius. The site, instrumentation, and flux calculation methodology have been described by *Bakwin et al.* [1998] and *Berger et al.* [2001]. Three-axis sonic anemometers at 30, 122, and 396 m above ground were used to measure turbulent winds and virtual potential temperature. Air from these three levels was drawn down tubes to a trailer where three LI-COR 6262 analyzers were used to determine CO_2 and water vapor mixing ratio fluctuations at 5 Hz for eddy covariance flux measurements [*Berger et al.*, 2001]. High-precision, 2-min mean CO_2 mixing ratios were sampled at 11, 30, 76, 122, 244, and 396 m by two LI-COR 6251 analyzers [*Bakwin et al.*, 1998]. Measurements of the NEE fluxes are described by *Davis et al.* [2003].

[5] A National Center for Atmospheric Research (NCAR) Integrated Sounding System (ISS), which includes a clear-air wind-profiling radar, a Radio Acoustic Sounding System (RASS), and a balloon-borne radiosonde system, was deployed about 8 km east of the tower from 15 March to 3 November 1998. The profiler is a sensitive 915 MHz Doppler radar that is designed to respond to fluctuations of the refractive index in clear air [*Ecklund et al.*, 1988; *White et al.*, 1991; *Angevine et al.*, 1994]. The reflectivity measured by the profiler is related to the turbulence intensity, gradients of temperature and humidity, and particulates [*Ottersten*, 1969; *Wyngaard and LeMone*, 1980; *White et al.*, 1991]. The ML depth (z_i) is derived from the signal-to-noise ratio (SNR) recorded by the profiler [*Yi et al.*, 2001]. The profiler can be used to measure z_i with a time resolution of 30 min or less, a height resolution of 60 to 100 m, a minimum height of 150 m, and a maximum height of 1500 to 3000 m depending on conditions [*Angevine et al.*, 1994]. ML depth cannot be estimated from the profiler SNR under unfavorable weather conditions such as rain, snow, or heavy clouds. The profiler is very sensitive to large cloud droplets and raindrops, resulting in a high, relatively featureless SNR over the depth of the precipitation shaft. Under these conditions, the boundary layer is often not clearly defined [*Stull*, 1988].

[6] Mixed layers shallower than 400 m, which typically occur in morning, are also not well defined from the profiler SNR measurements. The CO_2 mixing ratio measurements from the tower were used to obtain z_i when it was below 400 m. The top of the mixed layer was defined as the depth above ground to which the CO_2 mixing ratio is constant with height, provided that the net radiation is positive (warming the Earth's surface) [*Yi et al.*, 2001].

[7] The stable nocturnal ABL is typically very shallow, usually less than 200 m, and was estimated from the CO_2 measurements at the tower. We defined the top of the stable ABL as the height at which CO_2 gradients first become very small [*Yi et al.*, 2001]. The CO_2 mixing ratio measurements at the tower allowed us to estimate the stable ABL height for very stable and moderablely stable conditions as defined by *Mahrt et al.* [1998] and *Mahrt* [1999] but not for weakly stable conditions when the stable ABL height often exceeds 400 m.

2.2. Estimating the CO_2 Jump

[8] The CO_2 jump across the nocturnal inversion was determined from the difference in CO_2 mixing ratios between the nocturnal ABL and 396 m. The geometric height weighted average values were used as nocturnal ABL CO_2 mixing ratio. The nocturnal ABL height was estimated by visual examination of the CO_2 profile. We defined the top of the nocturnal ABL as the height at which the CO_2 mixing ratio was approximately equal to the mixing ratio in the residual boundary layer [*Yi et al.*, 2001]. We assumed that each CO_2 mixing ratio measurement represents a layer bounded by the midpoint between measurement heights. These layer edges were at 0, 20.5, 53, 99, 183, and 320 m, and layer thicknesses were 20.5, 32.5, 46, 84, and 137 m, respectively. Above the 200 m level, CO_2 mixing ratios are usually constant with time under stable conditions at night (e.g., see Figure 4 of *Yi et al.* [2001]). Therefore the CO_2 mixing ratio at 396 m at night can be considered typical of the residual layer. With disturbed weather conditions such as rain, snow, heavy clouds, or wind, the CO_2 mixing ratios at all six levels were similar and the CO_2 jump was very small.

[9] The CO_2 jump across the top of the ML can be estimated by the ML jump model [*Tennekes*, 1973; *Yi et al.*, 2001]:

$$\frac{d}{dt}\Delta C = \frac{\partial C}{\partial z}\frac{dz_i}{dt} - \frac{\partial C_m}{\partial t}, \tag{1}$$

$$\frac{\partial C_m}{\partial t} = \frac{1}{z_i}\left[(\overline{cw})_s - (\overline{cw})_i\right], \tag{2}$$

$$-(\overline{cw})_i = \Delta C\frac{dz_i}{dt}, \tag{3}$$

where C_m is the ML mean mixing ratio and ΔC is equal to $C_{FT} - C_m$. C_{FT} is the FT CO_2 concentration just above the ML, $(\overline{cw})$ is the eddy covariance flux of CO_2 (positive is an upward flux), subscript s and i refer to the surface and z_i, respectively, and $\partial C/\partial z$ is the mixing ratio gradient above the top of the ML. Three main approximations have been

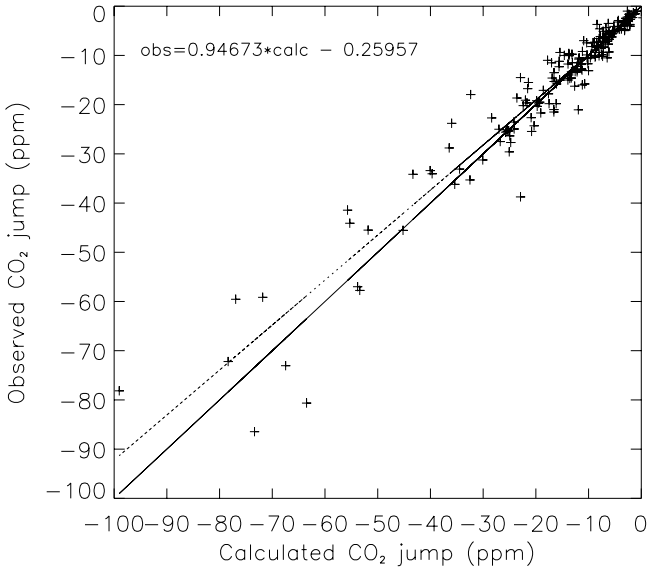

Figure 1. Hourly CO_2 jump between the ABL and the FT calculated by the mixed layer model vs. observed values. The data were limited to the morning period of ML growth when the ML top was below 396 m. The solid line is the 1:1 line and the dotted line is an orthogonal distance linear regression [*Press et al.*, 1992] (slope = 0.95).

made in the jump model in equations (1)–(3). First, the influence of mean vertical velocity on the entrainment of CO_2 into the ML is ignored. Synoptic vertical velocity is usually smaller than the entrainment velocity. We measured dz_i/dt [*Yi et al.*, 2001], which is actually a combination of entrainment velocity and the synoptic vertical velocity. Second, advection terms in equation (2) are neglected. The vertical advection is negligible everywhere except at the ML top because ML mixing ratios are nearly uniform in the vertical under convective conditions. However, significant horizontal transport of CO_2 could result from spatial gradients in CO_2 driven by different regional land cover patterns. Based on the tall tower observations, *Yi et al.* [2000] found that the relative contributions of total advection to NEE decreases with height. The monthly mean diurnal average daytime integral (from 0600 LT to 1800 LT) of total advection was estimated to be 2% of the daytime integral of NEE at 30 m. Thus, we ignored advection effects under well-mixed conditions.

[10] Combining equations (2) and (3), we get the CO_2 jump

$$\Delta C = \frac{z_i \dfrac{\partial C_m}{\partial t} - (\overline{cw})_s}{\dfrac{dz_i}{dt}}. \tag{4}$$

All terms on the right-hand side of equation (4) were measured from the tower and the ISS. The CO_2 mixing ratios at 11 m on the tower were used as C_m when the ML was shallow during the morning transition period ($z_i < 400$ m) and the average mixing ratios over six levels were used for the rest of the daytime ($z_i > 400$ m). The CO_2 fluxes measured at 30 m on the tower were used as $(\overline{cw})_s$. We note that equation (4) is only valid during the period when the ML is growing and it breaks down as z_i approaches its maximum value in the afternoon ($dz_i/dt \rightarrow 0$, $\Delta C \rightarrow \infty$).

[11] In the case of $dz_i/dt \rightarrow 0$, the solution of equation (1) can be expressed as

$$\Delta C(t) = \Delta C(t - \Delta t) - [C_m(t) - C_m(t - \Delta t)], \tag{5}$$

An increase in the ML mixing ratio leads to a decrease in the CO_2 jump. Thus when the ML reached maximum depth, the CO_2 jump was extrapolated with (5) from the tower mixing ratio measurements.

2.3. Direct Observations of the CO_2 Mixing Ratio Profile

[12] Shortly after sunrise, the ML begins to form near the ground with a relatively uniform CO_2 mixing ratio profile. When the ML is below 396 m, we define the CO_2 jump as the difference in CO_2 mixing ratio between the ML and 396 m [e.g., see *Yi et al.*, 2001, Figure 4]. As seen from Figure 1, the CO_2 jump calculated by the jump model during the morning hours is in good agreement with the direct observations from the tower.

[13] The CO_2 Budget and Rectification Airborne study (COBRA) [*Gerbig et al.*, 2003a, 2003b] measured vertical profiles of CO_2, H_2O, and potential temperature near the tower (Figure 2), thus providing a direct measurement of the CO_2 jump. The radar z_i measurements were consistent with the aircraft measurements in which the ML was defined to be a layer with nearly constant potential temperature (Figure 2b). The FT CO_2 values estimated by the jump model are in very good agreement with the aircraft measurements (Figure 2a). However, additional aircraft profiling suggests that the ability of the jump model in equations (1)–(5) to project the surface measurements to the FT is limited and this issue is discussed later in this section.

[14] Although only few hours were available to compare between the jump model and aircraft vertical profiles, the horizontal variability of the ML vertical profiles was clearly demonstrated by the aircraft measurements (Figure 2). These comparisons help in understanding the representativeness of the CO_2 jump estimated from the radar and tower measurements. Although in the ML, CO_2 is nearly constant with height, it varies horizontally as seen in Legs 1–2 in Figure 2a. Leg 2 may have higher ML CO_2 because it was near the shore of Lake Superior where there is little photosynthesis. Thus the CO_2 jumps computed at the WLEF tower may be influenced by local NEE of CO_2. The aircraft data (Figure 2) also indicate, as expected from previous studies of ABL structure, that the interface between the ML and FT is much more complicated than the simple step function assumed by the jump model [*Lily*, 1968; *Tennekes*, 1973; *Mahrt and Lenschow*, 1976; *Deardorff*, 1979].

[15] To further test the ability of the jump model and tower observations to determine the FT CO_2 mixing ratio, we compared our tower-based estimates with periodic aircraft profiling campaigns, mountaintop flask observations, and marine ABL flask observations (Table 2). It was evident that the amplitude of the seasonal CO_2 cycle in the FT estimated from the jump model is much larger than the observed upper tropospheric seasonal amplitude. This appears to contradict the good agreement found between the morning profiles (Figure 1) and COBRA profiles (Figure 2). The simplified

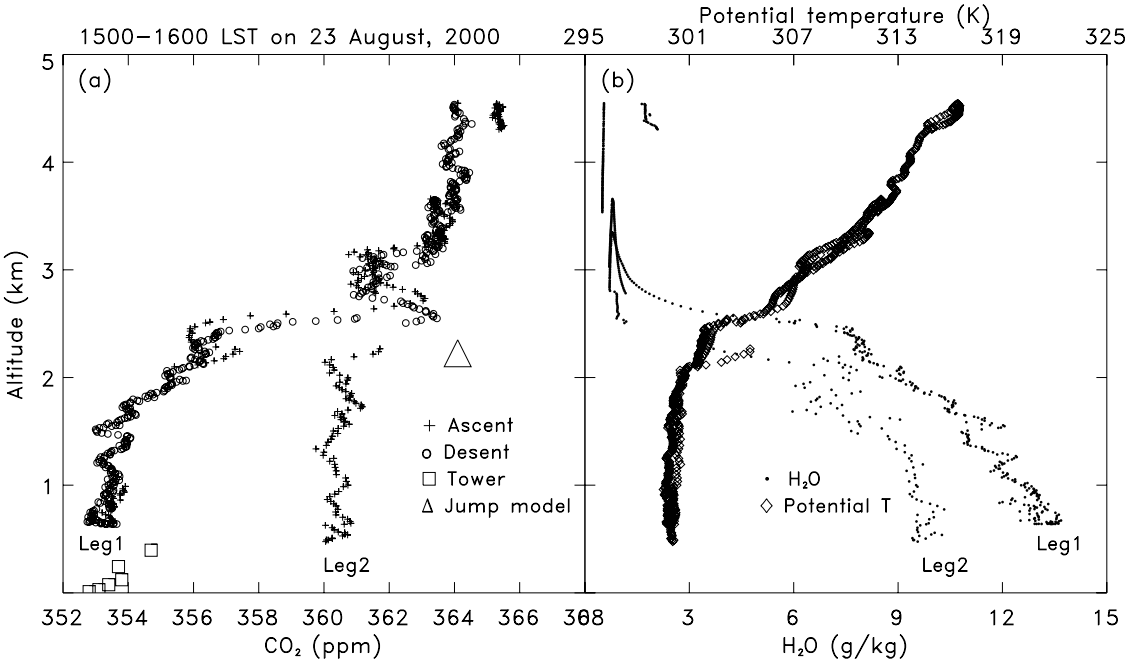

Figure 2. CO_2 concentrations in the ABL measured from the tower (square) and above the ABL estimated by the jump model (triangle plotted at the ML top as estimated from the ISS). Also plotted are aircraft measurements of CO_2 (plus and circle), H_2O (diamond), and potential temperature (period). The CO_2 mixing ratios and fluxes measured from the tower and the ML depths derived from 915-MHz radar SNR were used in the jump model. Leg 1 was around the tower and Leg 2 was near the shore of Lake Superior. The distance between these two legs is 181 km. The ML CO_2 difference between these two legs is about 7 ppm.

jump model in equations (1)–(3) assumes that C_{FT} is constant as a function of height just above the ML. The aircraft profiles show that C_{FT} was not constant with height. The vertical CO_2 gradients in the lower part of the FT were much larger than in the upper part of the FT (Figure 3). We hypothesize that the jump model calculation gave the mean CO_2 mixing ratio in the lower part of FT air that is in direct contact with the ML (e.g., the upper reaches of the ABL entrainment zone). The aircraft profiles support our assertion that the CO_2 jumps estimated by the jump model represent the difference between the ML and the lower FT (Figure 3). This difference was the reason why the seasonal variability of FT CO_2 estimated by the jump model and predicted by General Circulation Model (GCM) coupled with the Simple Biosphere Model (SiB2) was much larger than the direct measurements of the FT CO_2 mixing ratios (Table 2). The entrainment zone can be fairly deep [*Kiemle et al.*, 1997; *Davis et al.*, 1997], but the FT can still exhibit considerable vertical structure above the ABL (Figure 3a). As a result, jump model estimates of CO_2 in the FT were not always representative of the entire FT column. In fair weather conditions when the FT CO_2 mixing ratio appears fairly uniform subsidence compresses the troposphere (e.g., COBRA flights over Wisconsin), the jump model estimates appeared to capture the FT CO_2 mean mixing ratios fairly well. We chose to retain all jump model FT CO_2 estimates and compared these with the model-derived CO_2 mixing ratios in the lowest model layer above the ABL. For the sake of brevity, we hereafter refer to the results from the jump model driven by the direct measurements as "observations" and the results from the GCM with SiB2 as "simulations." Direct aircraft observations of FT CO_2 are explicitly differentiated from jump model estimates.

3. Results and Discussions

[16] We present comparisons between observations at WLEF and modeled fields, focusing on surface fluxes, ABL depths, and the jump in CO_2 between the ML and the lowest portion of the FT (as discussed above). The comparison is divided into the diurnal and seasonal averages in an effort to differentiate the temporal scales that drive the rectifier effect.

3.1. Diurnal Covariance

[17] The nocturnal CO_2 jump reached a maximum magnitude in the early morning (Figure 4) because CO_2 from

Table 1. Acronyms

Acronym	Explanation
ABL	Atmospheric boundary layer
COBRA	The CO2 Budget and Rectification Airborne Study
CSU	Colorado State University
FT	Free troposphere
GCM	General Circulation Model
ISS	Integrated Sounding System
MBL	Marine boundary layer
ML	Mixed layer
NEE	Net ecosystem-atmosphere exchange of CO_2
RASS	Radio Acoustic Sounding System
SNR	The signal-to-noise ratio
SiB2	The Simple Biosphere Model

Table 2. Comparison of Seasonal Variability of FT CO_2 Estimated by the Zero-Order Jump Model Driven by Surface Measurements to Direct Measurements

Site	Year	Seasonal Amplitude of FT CO_2, ppm	Comment
WLEF, WI (45.95°N)	1998	15.5	Estimated from a jump model driven by surface flux and ML profiling measurements (above the ML)
Model grid including WLEF, WI (45.95°N)	–	12.3	Above-ML CO_2 predicted by the CSU GCM with SiB2 [*Denning et al.*, 1995]
Marine boundary layer (MBL) (44.4°N)	1998	6.3	Including data from sites in both the Atlantic and Pacific Ocean basins [*Masarie and Tans*, 1995]
CARR, CO (40.9°N)	1993–2001	5.7	Aircraft measurements were between 4 and 8 km and data were detrended.
Niwot Ridge, CO (40.0°N)	1980–2000	5.6	A mountain site (3.5 km elevation)
Between Sendai (38°N) and Fukuoka (34°N), Japan	1979–2001	6.0	Aircraft measurements were between 4 and 8 km and data were detrended [*Nakazawa et al.*, 1993; and personal communication].

respiration accumulated in a shallow, stable ABL with weak mixing during the night. When the turbulent ML began to develop after sunrise, the CO_2 mixing ratio decreased rapidly owing to turbulent mixing, the entrainment of lower-CO_2 air from the above, photosynthesis, and possibly by advection [*Yi et al.*, 2000]. Solar radiation is the driving force for both photosynthesis and turbulent convection. At the time of the diurnal maximum of the ABL depth in the growing season (typically 1800–2000 m), the ML CO_2 mixing ratio was on average 1–6 ppm lower than aloft on average (Figures 4c–4f).

[18] We compared our observations with the Colorado State University (CSU) GCM coupled with the SiB2 [*Denning et al.*, 1996a, 1996b], which has a strong rectifier signal [*Denning et al.*, 1999]. For all months, the ML depths calculated by the simulation were less than we observed (Figure 4) and the GCM stable ABL depths were less than or equal to the observations. Underestimates of mixing depths and flux magnitudes had opposing effects on the CO_2 jump across the ABL top. The observed nocturnal CO_2 jump exceeded that of the simulation (Figure 4) with a maximum discrepancy of about 18 ppm in July. At midday during the growing season, the observations estimated the jump in CO_2 mixing ratio across the ABL top to be, on average, 1–6 ppm, while in the simulation, it was 1–3 ppm (Figures 4c–4f). Thus the simulation underestimated the diurnal covariance.

3.2. Seasonal Covariance

[19] Seasonal covariance plays a more important role in the rectifier effect than the diurnal covariance because seasonal changes are coherent and persistent across latitude zones [*Denning et al.*, 1996b]. To examine the seasonal covariance, we focused on the maximum daily ABL depth (from 1200 to 1600 LT) and daily integrated surface fluxes (24 hours). The day-to-day evolution of the afternoon ABL CO_2 mixing ratio reflects in part the daily integral of the surface fluxes. Rather than comparing the day-night mixing, flux, and mixing ratio differences, we contrasted the daily mean properties in the dormant season versus the growing season. Strong seasonal covariance would be characterized by shallow mixing and large respiration fluxes in dormant season and by deep mixing and large net photosynthetic fluxes in growing season. The observed seasonal distributions of maximum ABL depth, daily sum of CO_2 flux, and CO_2 jump are shown in Figure 5. The winter (December through February) ABL depth was shallowest (Figure 5a), but the largest CO_2 flux occurred in autumn (September through November) rather than in winter (Figure 5b).

[20] The simulated and observed net daily CO_2 fluxes were very similar (Figure 5b). Compared with WLEF observations, the simulated CO_2 fluxes were more positive in autumn and more negative in summer. Ecosystem respiration in the simulation was parameterized according to soil temperature and moisture and scaled to produce perfect carbon balance (NEE = 0) in the annual mean [*Denning et al.*, 1996a]. The simulated maximum ABL depths were too shallow throughout the year (Figure 5a). Undersimulated ABL depth should enhance the magnitude of the modeled CO_2 difference between the ABL and FT. The modeled CO_2 jump showed a persistent seasonal bias as compared to our tower-based observation (Figure 5c). The winter difference between simulation and observations therefore was consistent with the forcing variables. Similar fluxes but shallower modeled mixing yielded a larger magnitude CO_2 jump across the ABL top. The summer results for the CO_2 jump, however, contradicted the shallower modeled ABL depths. This may be related to an imperfect match between the observations and model output. Our observations did not include days with cloud convection which is common during the summer months and is an important mechanism for redistributing CO_2 in the atmosphere [*Hurwitz et al.*, 2004].

[21] Part of the discrepancy between the simulated and observed ABL thickness resulted from the definition of the ABL top in the GCM. The depth of the ABL is a prognostic variable in the model, which maintains the ABL top as a coordinate surface in order to resolve the jump in thermodynamic properties there [*Suarez et al.*, 1983; *Randall et al.*, 1992; *Denning et al.*, 1996b]. When the ABL becomes very deep, the model sacrifices vertical

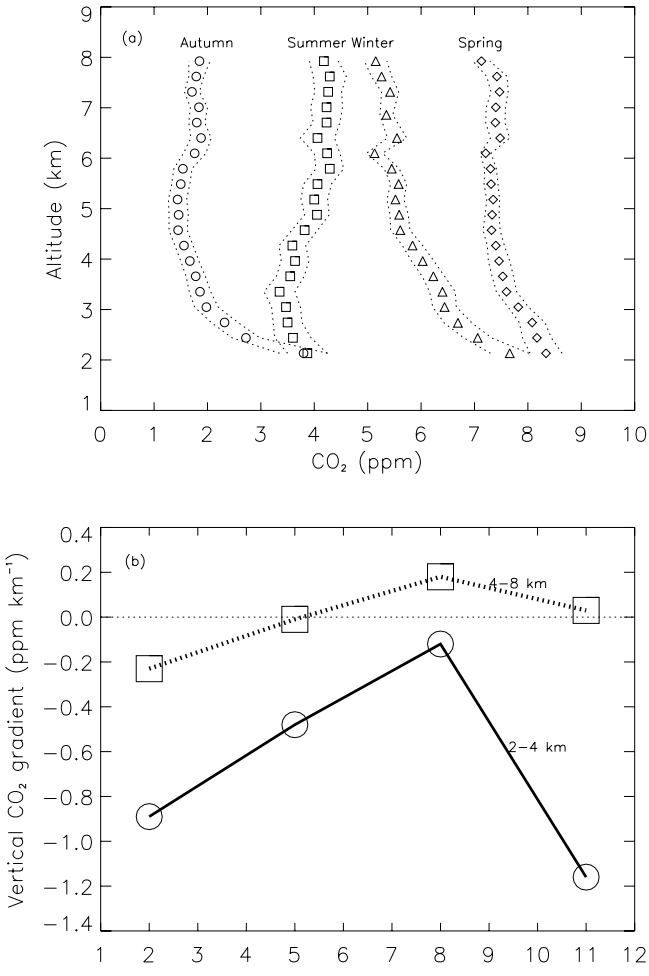

Figure 3. (a) Seasonal CO_2 vertical profiles from aircraft measurements over north central Colorado once a week (40.9 N, −104.8 W) from 1993 through 2001; (b) Seasonal CO_2 vertical gradients in lower part (solid line) and upper part (dotted line) of FT. These data were detrended by subtracting the linear regression values from the time series of data. The data points in Figure 3a are seasonal mean values for each height subtracted by 351 ppm. The dotted lines in Figure 3a indicate standard deviation of the mean. The seasonal amplitude of FT CO_2 (above 4 km) is about 5.7 ppm. Let $\delta C_{max} = C_{max} - C_{min}$, here C_{max} and C_{min} are maximum and minimum CO_2 mixing ratios above 4 km measured for each aircraft campaign, respectively. 70% of δC_{max} were within 2.3 ppm. The FT CO_2 is nearly constant above 4 km and has large variability below 4 km that is probably influenced by ABL mixing including clear-air convection (the ML) and shallow cumulus convection.

resolution near the surface to maintain the ability to resolve the jump. As a compromise to avoid this problem, a height of the mixed layer in the simulations reviewed here was restricted to be no deeper than 0.2 × (*ps* − 100 mb) (*ps* is surface pressure), which is generally about 1500 m, depending on temperature. On days when the ABL is deep, buoyancy and shear forcing in the ABL produce dry convective mixing with the layer above. A larger mass of air is in contact with the surface, which might correspond with the "real" ABL, but the coordinate surface at the simulated ABL is capped.

[22] The comparison between model and observation presented here is imperfect, and this introduces uncertainty in our conclusions. First, our observations were biased towards fair weather observing conditions. Owing to periods of poor observing conditions (rain, heavy cloud cover) and instrument failures, the measurements were available for only 40% of the deployed period of ISS. Under disturbed weather conditions the ABL may not be well defined, and we were often unable to identify the ML top using the radar or the stable ABL depth using the tower CO_2 profile. In the GCM, the top of the ABL was a model coordinate surface and was always defined. Also, the sonic anemometers used for CO_2 flux measurements did not operate well during rain.

[23] Second, our observations were a point measurement, while the results of the simulation represented a grid box (4° × 5°) average value. The comparison of observed and modeled ABL depths is not likely to suffer much from this mismatch of spatial scale, but it should be noted that the GCM grid box is much larger than the footprint of the tower CO_2 flux data [*Yi et al.*, 2000; *Davis et al.*, 2003].

4. Concluding Remarks

[24] Ecosystem CO_2 exchange and ABL mixing are correlated diurnally. Tracer transport models predict that these covariance signals produce a meridional gradient of annual mean CO_2 concentration in the MBL that is half as strong as the signal produced by fossil fuel emissions [*Denning et al.*, 1995, 1996b]. The effect of this covariance on MBL CO_2 mixing ratios has been identified as the CO_2 rectifier effect. It has been predicted by many inversion models [*Denning et al.*, 1995, 1996b; *Law and Simmonds*, 1996; *Law and Rayner*, 1999; *Bousquet et al.*, 2000; *Gurney et al.*, 2002, 2003]. However, observations to constrain the strength of these covariance signals in nature are lacking. We examined the strengths of these covariance signals in nature by using the measurements from the eddy flux tower, boundary layer profiling radar, and aircraft and compared the observations with that simulated by the CSU GCM with SiB2 [*Denning et al.*, 1996a, 1996b] at WLEF. We conclude that the observed diurnal and seasonal covariance between ecosystem CO_2 fluxes and ABL turbulent mixing are stronger than the global coupled model simulation. However, these results are subject to significant uncertainties associated with the use of a point measurement to represent an area and a fair weather bias in the data. The structure of FT CO_2 also confounds the comparison. Our study compared modeled and observed CO_2 differences between the ML and the lowest part of the FT. The column mean FT CO_2 mixing ratio is more relevant to the issue of the rectifier effect. Figure 3 shows that the vertical gradient in FT CO_2 is relatively small in summer and large and negative in the other months. Therefore the CO_2 difference between the ML and FT column mean would be more similar to that measured by the jump model in summer, but larger (more negative) in the other months. This implies that the seasonal rectifier forcing could be possibly larger than

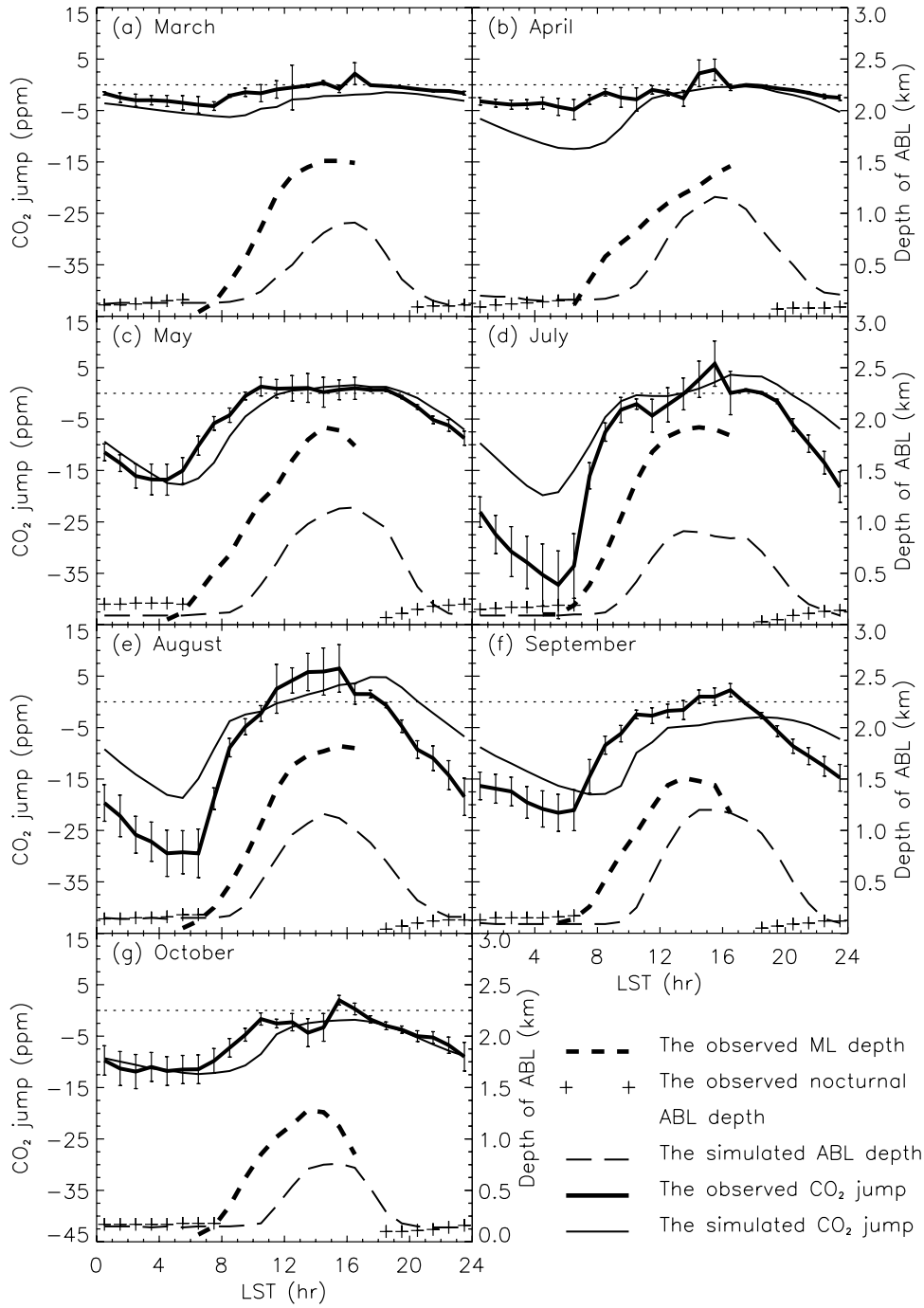

Figure 4. Monthly mean diurnal cycle of mixed layer depth (thick dashed line for observations and long dashed line for simulation [*Denning et al.*, 1996b]), stable layer depth (plus for observations and long dashed line for simulation) and CO_2 jump across the top of ABL (solid line with standard error bars for observations and without error bars for simulation) for 1998. The days represented in the observations are those for which we could identify the ABL top, and days when radar, CO_2 flux and mixing ratio instruments were all functioning. This represents 40% of the available days between March and October, not including June, which is absent due to missing data.

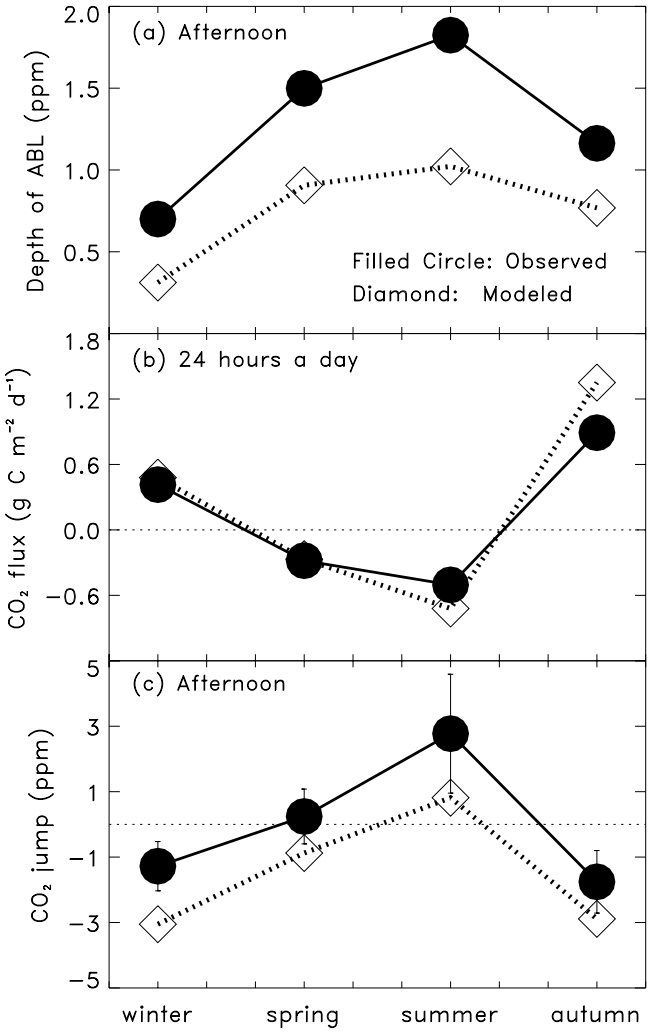

Figure 5. Comparison of seasonal distributions of simulated [*Denning et al.*, 1996b] (dotted lines) with observed (solid line) (a) maximum ABL depth, (b) daily integral of the surface CO_2 flux, and (c) CO_2 jump. The mixed layer depths for January, February, November, and December were estimated from an empirical formula [*Yi et al.*, 2001] driven by measurements of the surface virtual potential temperature flux. Standard errors are plotted in Figure 5c for the observations. The "Afternoon" in Figures 5a and 5c refers to the period during which the ML attains maximum depth and begins at 1200 and ends at 1600 LT.

that estimated from the jump model results. Modeled column mean FT CO_2 was not analyzed in this study.

[25] **Acknowledgments.** This work was supported in part by the Biological and Environmental Research Program (BER), U.S. Department of Energy, under grant DOE/DE-FG02-97ER62457, a contribution to the joint program on Terrestrial Ecology and Global Change, and in part by the Biological and Environmental Research Program (BER), U.S. Department of Energy, through the Great Plains Regional Center of the National Institute for Global Environmental Change (NIGEC) under Cooperative Agreement DE-FC03-90ER61010. NCAR's Atmospheric Technology Division managed the field deployment and operation of the NCAR Integrated Sounding System. Financial support for the ISS came from NCAR/ATD's instrument deployment pool. Work at the WLEF tower was supported by in part by the Atmospheric Chemistry Project of the Climate and Global Change Program of the National Oceanic and Atmospheric Administration and by the Department of Energy's National Institutes for Global Environmental Change regional center at Indiana University. Field support for the ISS was provided by the USDA Forest Service Forest Sciences Laboratory in Rhinelander, Wisconsin, courtesy of Jud Isebrands and Ron Teclaw. Bruce Cook (U. Minnesota) provided additional field support. We thank Steven Wofsy (Harvard U.) for his comments on a draft of this paper, and Ron Teclaw (USDA-FS) and Conglong Zhao (U. Colorado/CIRES) for their support of the WLEF tower instrumentation. The constructive comments of three anonymous reviewers are gratefully acknowledged. We also thank the State of Wisconsin Educational Communications Board for use of the transmitter tower facilities and R. Strand (Park Falls, WI) for invaluable assistance enabling effective work at the tower.

References

Angevine, W. M., A. B. White, and S. K. Avery (1994), Boundary-layer depth and entrainment zone characterization with a boundary-layer profiler, *Boundary Layer Meteorol.*, *68*, 375–385.

Angevine, W. M., P. S. Bakwin, and K. J. Davis (1998), Wind profiler and RASS measurements compared with measurements from a 450-m tall tower, *J. Atmos. Ocean. Technol.*, *15*, 818–825.

Bakwin, P. S., P. P. Tans, D. F. Hurst, and C. Zhao (1998), Measurements of carbon dioxide on very tall towers: Results of the NOAA/CMDL program, *Tellus*, *50B*, 401–415.

Baldocchi, D., et al. (2001), Fluxnet: A new tool to study the temporal and spatial variability of ecosystem-scale carbon dioxide, water vapor, and energy flux densities, *Bull. Am. Meteorol. Soc.*, *82*, 2415–2434.

Berger, B. W., K. J. Davis, C. Yi, P. S. Bakwin, and C. Zhao (2001), Long-term carbon dioxide fluxes from a very tall tower in a northern forest: Flux measurement methodology, *J. Ocean. Atmos. Technol.*, *18*, 529–542.

Bousquet, P., P. Peylin, P. Ciais, C. L. Quere, P. Friedlingstein, and P. P. Tans (2000), Regional changes in carbon dioxide fluxes of land and oceans since 1980, *Science*, *290*, 1342–1346.

Conway, T. J., P. Tans, L. S. Waterman, K. W. Thoning, D. R. Kitzis, K. A. Masarie, and N. Zhang (1994), Evidence for interannual variability of the carbon cycle from the National Oceanic and Atmospheric Administration/Climate Monitoring and Diagnostics Laboratory Global Air Sampling Network, *J. Geophys. Res.*, *99*, 22,831–22,855.

Davis, K. J., D. H. Lenschow, S. P. Oncley, C. Kiemle, G. Ehret, and A. Giez (1997), The role of entrainment in surface-atmosphere interactions over the boreal forest, *J. Geophys. Res.*, *102*, 29,219–29,230.

Davis, K. J., P. S. Bakwin, C. Yi, B. W. Berger, C. Zhao, R. Teclaw, and J. Isebrands (2003), The annual cycle of net CO_2 and H_2O exchange over a northern mixed forest as observed from a very tall tower, *Global Change Biol.*, *9*, 1278–1293.

Deardorff, J. W. (1979), Prediction of convective mixed-layer entrainment for realistic capping inversion structure, *J. Atmos. Sci.*, *36*, 424–436.

Denning, A. S., I. Y. Fung, and D. Randall (1995), Latitudinal gradient of atmospheric CO_2 due to seasonal exchange with land biota, *Nature*, *376*, 240–243.

Denning, A. S., G. J. Collatz, C. Zhang, D. A. Randall, J. A. Berry, P. J. Sellers, G. D. Collello, and D. A. Dazlich (1996a), Simulations of terrestrial carbon metabolism and atmospheric CO_2 in a general circulation model, part 1, Surface carbon fluxes, *Tellus*, *48B*, 521–542.

Denning, A. S., D. A. Randall, G. J. Collatz, and P. J. Sellers (1996b), Simulations of terrestrial carbon metabolism and atmospheric CO_2 in a general circulation model, part 2: Simulated CO_2 concentration, *Tellus*, *48B*, 543–567.

Denning, A. S., T. Takahashi, and P. Friedlingstein (1999), Can a strong atmospheric CO_2 rectifier effect be reconciled with a "reasonable" carbon budget?, *Tellus*, *51B*, 249–253.

Ecklund, W. L., D. A. Carter, and B. B. Balsley (1988), A UHF wind profiler for the boundary layer: Brief description and initial results, *J. Atmos. Ocean. Technol.*, *5*, 432–441.

Gerbig, C., J. C. Lin, S. C. Wofsy, B. C. Daube, A. E. Andrews, B. B. Stephens, P. S. Bakwin, and C. A. Grainger (2003a), Toward constraining regional-scale fluxes of CO_2 with atmospheric observations over a continent: 1. Observed spatial variability from airborne platforms, *J. Geophys. Res.*, *108*(D24), 4756, doi:10.1029/2002JD003018.

Gerbig, C., J. C. Lin, S. C. Wofsy, B. C. Daube, A. E. Andrews, B. B. Stephens, P. S. Bakwin, and C. A. Grainger (2003b), Toward constraining regional-scale fluxes of CO_2 with atmospheric observations over a continent: 2. Analysis of COBRA data using a receptor-oriented framework, *J. Geophys. Res.*, *108*(D24), 4757, doi:10.1029/2003JD003770.

Gurney, K. R., et al. (2002), Towards robust regional estimates of CO_2 sources and sinks using atmospheric transport models, *Nature*, *415*, 626–630.

Gurney, K. R., et al. (2003), TransCom3 CO_2 inversion intercomparison: 1. Annual mean control results and sensitivity to transport and prior flux information, *Tellus*, *55B*, 555–579.

Hurwitz, M. D., D. M. Ricciuto, K. J. Davis, W. Wang, C. Yi, M. P. Butler, and P. S. Bakwin (2004), Advection of carbon dioxide in the presence of storm systems over a northern Wisconsin forest, *J. Atmos.*, in press.

Kiemle, C., G. Ehret, A. Giez, K. J. Davis, D. H. Lenschow, and S. P. Oncley (1997), Estimation of boundary-layer humidity fluxes and statistics from airborne DIAL, *J. Geophys. Res.*, *102*, 29,189–29,204.

Law, R. M., and P. J. Rayner (1999), Impacts of seasonal covariance on CO_2 inversions, *Global Biogeochem. Cycles*, *13*, 845–856.

Law, R. M., and I. Simmonds (1996), The sensitivity of deduced CO_2 sources and sinks to variations in transport and imposed surface concentrations, *Tellus*, *48B*, 613–625.

Law, R. M., et al. (1996), Variations in modelled atmospheric transport of carbon dioxide and the consequences for CO_2 inversions, *Global Biogeochem. Cycles*, *10*, 783–796.

Lily, D. K. (1968), Models of cloud-toped mixed layer under strong inversion, *Q. J. R. Meteorol. Soc.*, *94*, 292–309.

Mahrt, L. (1999), Stratified atmospheric boundary layers, *Boundary Layer Meteorol.*, *90*, 375–396.

Mahrt, L., and D. H. Lenschow (1976), Growth dynamics of the convectively mixed layer, *J. Atmos. Sci.*, *33*, 41–51.

Mahrt, L., J. Sun, W. Blumen, T. Delany, and S. Oncley (1998), Nocturnal boundary-layer regimes, *Boundary Layer Meteorol.*, *88*, 255–278.

Masarie, K. A., and P. P. Tans (1995), Extension and integration of atmospheric carbon dioxide data into a globally consistent measurement record, *J. Geophys. Res.*, *100*, 11,593–11,610.

Nakazawa, T., S. Morimoto, S. Aoki, and M. Tanaka (1993), Time and space variations of the carbon isotopic ratio of tropospheric carbon dioxide over Japan, *Tellus*, *45B*, 258–274.

Ottersten, H. (1969), Atmospheric structure and radar backscattering in clear air, *Radio Sci.*, *4*, 1179–1193.

Press, W. H., S. A. Teukolsky, W. T. Vettering, and B. P. Flannery (1992), *Numerical Recipes in C*, 2nd ed., Cambridge Univ. Press, New York.

Randall, D. A., Q. Shao, and C.-H. Moeng (1992), A second-order bulk boundary-layer model, *J. Atmos. Sci.*, *49*, 1903–1923.

Stull, R. B. (1988), *An Introduction to Boundary-Layer Meteorology*, 666 pp., Kluwer Acad., Norwell, Mass.

Suarez, M. J., A. Arakawa, and D. A. Randall (1983), Parameterization of the planetary boundary layer in the UCLA general circulation model: Formulation and results, *Mon. Weather Rev.*, *111*, 2224–2243.

Tans, P. P., I. Y. Fung, and T. Takahashi (1990), Observational constraints on the global atmospheric CO_2 budget, *Science*, *247*, 1431–1438.

Tennekes, H. (1973), A model for the dynamics of the inversion above a convective boundary layer, *J. Atmos. Sci.*, *30*, 558–567.

White, A. B., C. W. Fairall, and D. W. Thompson (1991), Radar observations of humidity variability in and above the marine atmospheric boundary layer, *J. Atmos. Ocean. Technol.*, *8*, 639–658.

Wyngaard, J. C., and M. A. LeMone (1980), Behavior of the refractive index structure parameter in the entraining convective boundary layer, *J. Atmos. Sci.*, *37*, 1573–1585.

Yi, C., K. J. Davis, B. W. Berger, and P. B. Bakwin (2001), Long-term observations of the dynamics of the continental planetary boundary layer, *J. Atmos. Sci.*, *58*, 1288–1299.

Yi, C., K. J. Davis, P. B. Bakwin, B. W. Berger, and L. C. Marr (2000), The influence of advection on measurements of the net ecosystem-atmosphere exchange of CO_2 from a very tall tower, *J. Geophys. Res.*, *105*, 9991–9999.

P. S. Bakwin, NOAA Climate Monitoring and Diagnostics Laboratory, 325 Broadway, Boulder, CO 80305, USA. (pbakwin@comcast.net)

K. J. Davis, A. Desai, and C. Yi, Department of Meteorology, Pennsylvania State University, University Park, PA 16802, USA. (davis@essc.psu.edu; adesai@essc.psu.edu; cxyi@essc.psu.edu)

A. S. Denning and N. Zhang, Department of Atmospheric Science, Colorado State University, Fort Collins, CO 80523-1371, USA. (denning@atmos.colostate.edu; ni@dendrus.atmos.colostate.edu)

C. Gerbig and J. C. Lin, Department of Earth and Planetary Sciences, Harvard University, Cambridge, MA 02138, USA. (chg@io.harvard.edu; johnlin@fas.harvard.edu)